11th World Congress on Computational Mechanics (WCCM XI)
5th European Conference on Computational Mechanics (ECCM V)
6th European Conference on Computational Fluid Dynamics (ECFD VI)
E. Oñate, J. Oliver and A. Huerta (Eds)

AN UNSTEADY SHOCK-FITTING TECHNIQUE FOR UNSTRUCTURED GRIDS

A. BONFIGLIOLI[*], R. PACIORRI[†] AND L. CAMPOLI[†]

[*] Scuola di Ingegneria
Università degli Studi della Basilicata
Viale dell'Ateneo Lucano 10, 85100 Potenza, Italy
e-mail: aldo.bonfiglioli@unibas.it, web page: http://www.unibas.it/

[†] Dipartimento di Ingegneria Meccanica e Aerospaziale (DIMA)
Università di Roma, La Sapienza
Via Eudossiana 18, 00184 Roma, Italy
e-mail: renato.paciorri@uniroma1.it - Web page: http://http://www.dima.uniroma1.it/dima/

Key words: Shock-capturing, Shock-fitting, Arbitrary Lagrangian Eulerian, Moving Grids, Unsteady flows

Abstract. A novel, unstructured, shock-fitting algorithm capable of simulating steady flows has being further developed to make it capable of dealing with un-steady flows. The present paper discusses and analyses the early efforts made to extend to *unsteady* flows the existing algorithm. The properties of the unsteady version of this novel unstructured shock-fitting technique are tested by reference to a simple, but not trivial, test case that confirms that the proposed shock-fitting technique preserves second-order accuracy downstream of a moving shock wave.

1 INTRODUCTION

In recent years, the authors have developed an unstructured, shock-fitting algorithm capable of simulating *steady* flows in two [1, 2] and three [3] spatial dimensions. The fitted shocks are treated as interior boundaries of zero thickness that are free to move throughout a triangular/tetrahedral mesh that covers the entire computational domain and locally adapts to follow the shock motion. The Rankine–Hugoniot jump relations are used to compute the Lagrangian motion of the discontinuities and the unstructured, shock-capturing solver described in [4] is used to discretise the governing PDEs in the smooth regions of the flow-field.

The aforementioned methodology is being further developed to make it capable of dealing with un-steady flows. This can be accomplished by introducing three new ingredients:

i) the shock-capturing code must be capable of working in an Arbitrary Lagrangian Eulerian (ALE) setting; *ii*) the order of accuracy of the Lagrangian shock motion must be raised to second order; and *iii*) the algorithm must be capable of automatically detecting changing flow topologies, such as those that occur when a shock meets another shock or a solid wall.

The former two issues are addressed in this paper, whereas the latter is left for future work. Because of this, the current version of the unstructured, shock-fitting algorithm can only be used to simulate un-steady flows that do not undergo topological changes. Its current capabilities are demonstrated by reference to a piston-driven flow: the moving shock wave generated by a piston which is impulsively set into motion interacts with the expansion that forms once the piston starts decelerating. This one-dimensional, un-steady problem is solved on a truly unstructured two-dimensional planar grid.

The analysis of the numerical results shows that the proposed shock-fitting methodology is capable of computing high quality solutions of unsteady flows with shocks while preserving the design order of accuracy of the fluid dynamic solver also in the region downstream of the moving shock.

2 NUMERICAL METHOD

The unstructured shock-fitting algorithm consists of two key ingredients: 1) a local re-meshing technique that constructs a time-dependent mesh in which the fitted discontinuities are internal boundaries of zero thickness and 2) an algorithm for solving the Rankine–Hugoniot jump relations that provide the Lagrangian velocity of the discontinuity and an updated set of dependent variables within the downstream side of the fitted shock.

More precisely, in two space dimensions, the fitted shock fronts are made of polygonal curves, i.e., a connected series of line segments (which we call the shock edges) that join the shock points. These shocks are free to move throughout a background triangular mesh that covers the entire computational domain, see Fig. 1(a).

At a given time level n, a local, constrained Delaunay triangulation is applied in the neighbourhood of the shock front to ensure that the edges that make up the shock front are also part of the triangular grid that covers the entire computational domain, see Fig. 1(b).

The shock speed and downstream state are computed according to the Rankine–Hugoniot jump relations and each of the shock points is moved in a Lagrangian manner, see Fig. 1(c). A more detailed description of the shock-fitting algorithm can be found in [1, 2].

It is important to underline that the shock-fitting algorithm described in aforementioned references is only capable of accurately computing steady flows. There are two reasons for this.

First, it does not take into account that the triangular cells that abut on the shock front have one of their edges that moves with the shock, thus deforming the cell. This

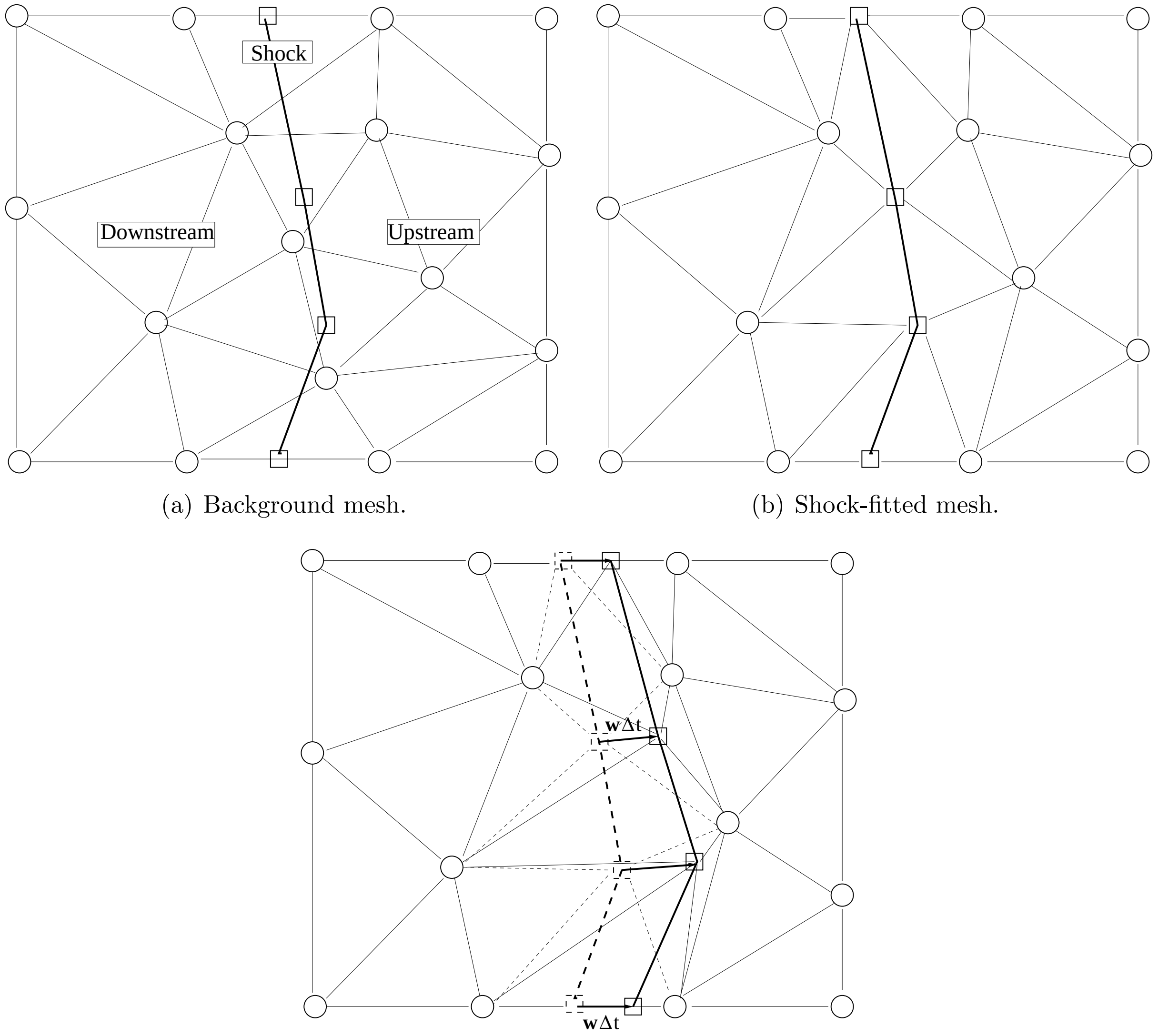

(a) Background mesh.

(b) Shock-fitted mesh.

(c) Shock motion and cell deformation.

Figure 1: Shock-fitting algorithm: mesh evolution during shock motion.

is schematically shown in Fig. 1(c) where dashed lines are used to show the edges of the triangular cells when the shock front is at time level n and solid lines to show the same sides when the shock has reached time level $n + 1$.

Second, the position P_i of the shock points is updated using the first-order-accurate Euler explicit scheme:

$$P_i^{n+1} = P_i^n + w_{sh}^n \Delta t$$

where w_{sh}^n is the shock speed evaluated at time level n and Δt is the time step size.

Ignoring the deformation of the cells and using a first-order-accurate formula for computing the shock trajectory does not affect the correctness and the spatial accuracy of

Table 1: Inviscid vortex convected by a supersonic stream: L_2-norm of the discretization error and measured order of convergence.

grid		$\sqrt{\rho}$		$\sqrt{\rho}H$		$\sqrt{\rho}u$		$\sqrt{\rho}v$	
level	$\Delta t\, U_\infty/L$	L_2	$\tilde{n}$	L_2	$\tilde{n}$	L_2	$\tilde{n}$	L_2	$\tilde{n}$
1	.0147902	0.1255E-01	-	0.2843E-01	-	0.2289E-01	-	0.3052E-01	-
2	.0073951	0.6002E-02	1.06	0.1275E-01	1.16	0.9630E-02	1.25	0.1376E-01	1.15
3	.0036975	0.1863E-02	1.69	0.3725E-02	1.78	0.2839E-02	1.76	0.4139E-02	1.73
4	.0018488	0.4886E-03	1.93	0.9512E-03	1.97	0.7179E-03	1.98	0.1072E-02	1.95
5	.0009244	0.1228E-03	1.99	0.2361E-03	2.01	0.1780E-03	2.01	0.2691E-03	1.99

steady state calculations, but completely jeopardise the computation of un-steady solutions. Therefore, the minimum requirements for making time-accurate the steady version of the shock-fitting algorithm consist in implementing an ALE technique in the gas-dynamic solver and a second-order-accurate time integration of the shock trajectory.

The shock-capturing solver described in [4] now uses the second-order-accurate (in both space and time) ALE Lax-Wendroff (LW) scheme described in [5]. Discrete conservation and the fulfilment of the Geometric Conservation Law is accomplished as described in [6].

The spatial and temporal accuracy of the ALE-LW scheme has been verified using an exact solution of the un-steady Euler equations which consists in a vortex convected by a uniform stream, see [7]. Starting from a coarse Delaunay grid and time-step length, five levels of nested grids have been created by recursive subdivision of the coarsest one. The time-step length has also been halved when passing from a given grid level to the finer one. The mesh expands and then shrinks while the vortex is convected over a distance approximately equal to 1.5 times the vortex size. Table 1 shows the L_2-norm of the discretization error at the final time for each component of Roe's parameter vector along with a global measure of the order-of-convergence ($\tilde{n}$) for each pair of consecutive grid levels; it can be seen that design order is recovered.

The order of accuracy of the shock trajectory has been raised to second order by implementing a two-steps time integration scheme. More specifically, the predictor step estimates the position of the shock at time level $n + 1/2$ using the explicit Euler scheme:

$$P_i^{n+1/2} = P_i^n + w_{sh}^n \Delta t/2.$$

The shock speed $w_{sh}^{n+1/2}$ at time level $n + 1/2$ is then computed using the intermediate shock position $P_i^{n+1/2}$ and, finally, the position of each shock point is updated at time level $n + 1$ in the corrector step:

$$P_i^{n+1} = P_i^n + w_{sh}^{n+1/2} \Delta t.$$

3 TEST-CASE

In order to assess the properties of this novel unsteady shock-fitting technique, a simple, but not trivial, test-case has been numerically simulated. A planar, piston-cylinder assembly is initially filled with air (treated as an inviscid, perfect gas) at rest. The piston, which bounds the cylinder on its left end, is impulsively set into motion with speed $v_p/a_1 = 0.735$, a_1 being the isothermal speed of sound ($a = \sqrt{RT}$) of the quiescent air. The evolution of the flow is sketched in the $x - t$ plane in Fig. 2: a moving shock wave is generated, which travels towards the closed (right) end of the cylinder. At time $t\,a_1/L = 0.24$, the velocity of the piston starts decreasing until it stops; a continuous expansion wave is generated which reaches the shock, thus reducing its strength and speed.

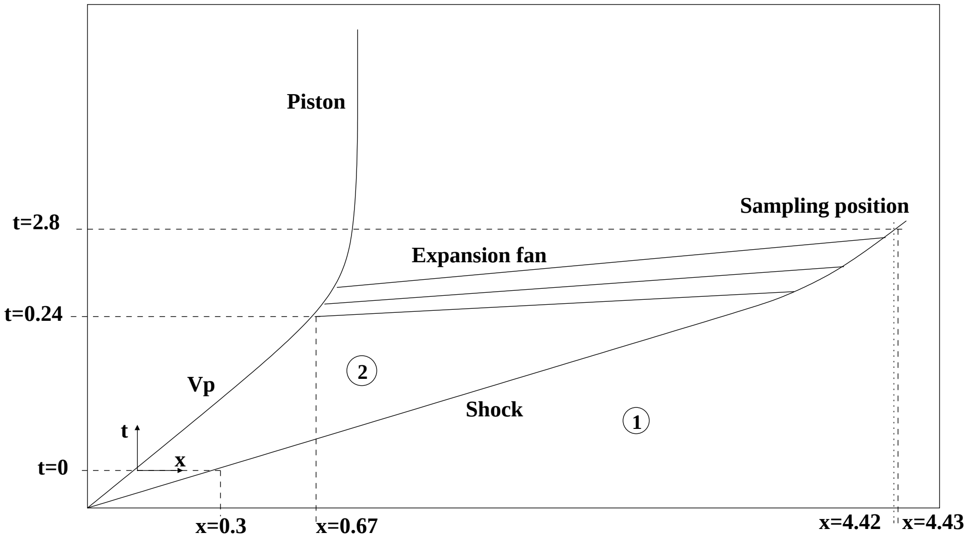

Figure 2: Unsteady, piston-driven flow: evolution in the space-time plane.

When the numerical simulation begins at $t = 0$, the computational domain is a rectangle having dimensions $5L \times L$ in the stream-wise and cross-flow directions and the shock wake has already travelled a distance $x/L = 0.3$ to the right of the piston. With reference to Fig. 2, the initial states, respectively upstream and downstream of the moving shock, are denoted as 1 and 2 and are reported in Tab. 2. The simulation is run up to a final time $t\,a_1/L = 2.8$. At this time, the shock is at $x/L = 4.43$ and has almost reached the closed (right) end of the cylinder. Even though this test case could be simulated using a one-dimensional flow model, the numerical simulation has been performed on a two-dimensional mesh. This background mesh is made of 6369 grid-points and 12448 triangular elements and the shock front has been discretised using 41 shock points. The background mesh has been generated so as to avoid any alignment among the cell edges and the wave fronts so that the numerical simulation is truly two-dimensional. The computational domain is shown in Fig. 3(a), where the computational mesh in the region surrounding the shock front at $ta_1/L = 2.8$ is shown in detail. During time evolution, the

Table 2: Unsteady, piston-driven flow: initial states.

state	a/a_1	p/p_1	u/a_1
1	1	1	0
2	1.159	2.2577	0.735

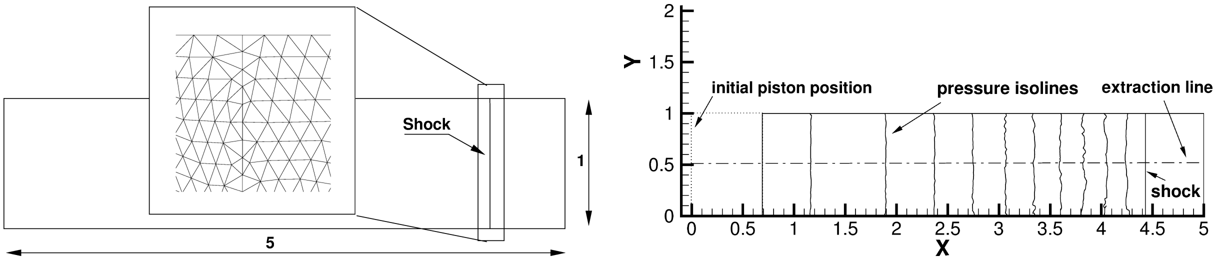

(a) Detail of the mesh in the neighbourhood of the shock.

(b) Pressure iso-contours at $t = 2.8$.

Figure 3: Unsteady, piston-driven flow: computational mesh and pressure iso-contours.

stream-wise size of the computational domain is reduced because of the piston's motion. All nodes of the background mesh move as the time elapses, but the topology of the mesh does not change. Therefore, at each integration step, all the cells of the computational mesh are deformed and not only those in the neighbourhood of the shock.

4 COMPUTATIONAL RESULTS

Figure 3(b) shows the pressure iso-contours at time $t\, a_1/L = 2.8$ computed by the shock-fitting solver. The structure of the flow field is rather simple. The shock wave divides the computational domain into two regions: the upstream region (on the right) where the gas is at rest and the downstream region where flow is not uniform due to the expansion caused by the piston's deceleration.

Figure 4(a) shows the temporal evolution of the pressure ratio (p/p_1) inside the cylinder as the piston proceeds in its motion. These pressure distributions were extracted along the line shown in Fig. 3(b) at subsequent time instants, uniformly spaced apart ($\Delta t\, a_1/L = 0.2$). The position of the shock wave can be clearly seen at all the times because of the pressure jump. The effects of the expansion fan on the shock wave strength are also evident. Indeed, the pressure jump decreases continuously as the shock moves towards the right end of the cylinder. The spurious disturbances that can be seen in Figs. 3(b) and 4(a) on the pressure distributions are the effect of the numerical error and are related to the two-dimensional nature of the simulation. Indeed, since the grid is truly unstructured, the edges of the triangles and the wave fronts are everywhere mis-aligned, so that cross-flow variations inevitably arise.

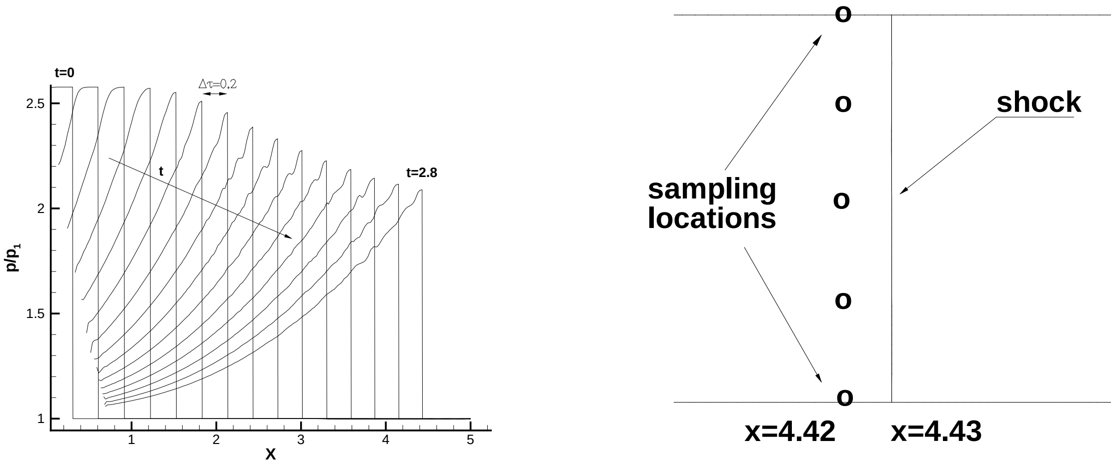

(a) Pressure ratio time-history.

(b) Sampling points used in the temporal grid-convergence analysis.

Figure 4: Unsteady, piston-driven flow.

Table 3: Unsteady, piston-driven flow: pointwise, observed order of time accuracy.

y	ϕ_1	ϕ_2	ϕ_3	n
0.0000	1.48912	1.48963	1.48975	2.0875
0.2739	1.48995	1.49123	1.49155	2.0000
0.5746	1.49602	1.49702	1.49727	2.0001
0.7514	1.49804	1.49828	1.49833	2.2630
1.0000	1.49702	1.49805	1.49827	2.2271

In order to assess the order of time accuracy of the unstructured, shock-fitting algorithm, the Richardson extrapolation technique described in [8] has been used. Using a given spatial resolution, three different time step lengths have been considered, namely: $\triangle t_1 = 2\triangle t_2$ and $\triangle t_2 = 2\triangle t_3$, with $\triangle t_3\, a_1/L = 0.001$. The observed order of accuracy (n) in time is obtained pointwise via the following relation:

$$n = \frac{\log\left(\frac{\phi_1-\phi_2}{\phi_2-\phi_3}\right)}{\log\left(2\right)}$$

where ϕ represents a generic variable and the subscripts refer to the solutions computed with different time step lengths Δt. In the present analysis, $\phi = \sqrt{\rho}$ and the solutions at $t\, a_1/L = 2.8$ were sampled at five different locations at $x/L = 4.42$, i.e. immediately downstream of the shock wave, see Fig. 4(b). The y coordinate of the sampling locations, the values ϕ_i and the pointwise values of the observed order of accuracy are reported in Table 3.

Table 3 clearly shows that the order of accuracy downstream of the shock is very close to the formal order of the gas-dynamic solver, i.e. second order. This result highlights one of the key advantages of shock-fitting vs. shock-capturing: shock-fitting is capable of preserving the formal order of accuracy of the gas-dynamic solver in the region downstream of a shock wave.

5 CONCLUSIONS

A preliminary version an unsteady, shock-fitting technique for unstructured grids has been successfully developed. The current version allows to simulate flows with moving shocks, but it does not allow to deal with topological changes in the shock structure. The capability of automatically identifying changing topologies will be subject of future work. To accomplish this non-trivial task, the authors have recently [9] started investigating the use of fuzzy logic and pattern recognition algorithms originally developed in image analysis.

REFERENCES

[1] Paciorri, R. and Bonfiglioli, A. A Shock-Fitting Technique for 2D Unstructured Grids. *Computers & Fluids* (2009) **38**:715–726

[2] Paciorri, R. and Bonfiglioli, A. Shock Interaction Computations on Unstructured, Two-Dimensional Grids Using a Shock-Fitting Technique. *J. of Comp. Physics* (2011) **230**:3155–3177.

[3] Bonfiglioli, A. and Grottadaurea, M. and Paciorri, R. and Sabetta, F. An Unstructured, Three-Dimensional, Shock-Fitting Solver for Hypersonic Flows. *Computers & Fluids* (2013) **73**:162–174.

[4] Bonfiglioli, A. Fluctuation Splitting Schemes for the Compressible Fluctuation and Incompressible Euler and Navier–Stokes Equations. *Int. J. of Comp. Fluid Dynamics* (2000) **14**:21–39.

[5] Lefrançois, E. and Dhatt, G. and Vandromme, D. Fluid–structural interaction with application to rocket engines. *Int. J for Num. Methods in Fluids* (1999) **30**:865–895

[6] Michler, C. and De Sterck, H. and Deconinck, H. An arbitrary Lagrangian Eulerian formulation for residual distribution schemes on moving grids. *Computers & Fluids* (2003) **32**:59-71.

[7] Bonfiglioli, A. and Paciorri, R. (2013) A mass-matrix formulation of unsteady fluctuation splitting schemes consistent with Roe's parameter vector. *Int. J. of CFD* **27**:210–227

[8] Roache, P. Quantification of uncertainty in computational fluid dynamics. *Ann. Review of Fluid Mechanics* (1997) **29**:123–160.

[9] Paciorri, R. and Bonfiglioli, A. Recognition of shock-wave patterns from shock-capturing solutions. *Computational modelling of Objects represented in Images.* CRC Press, (2012) 91-96